IOP Publishing Journal of Physics G: Nuclear and Particle Physics
J. Phys. G: Nucl. Part. Phys. **47** (2020) 035108 (15pp) https://doi.org/10.1088/1361-6471/ab6627

Effects of impact parameter filters on observables in heavy-ion collisions at INDRA energies

Pengcheng Li[1,2], Yongjia Wang[2,5], Qingfeng Li[2,3,5], Jiansong Wang[2,3] and Hongfei Zhang[1,4]

[1] School of Nuclear Science and Technology, Lanzhou University, Lanzhou 730000, People's Republic of China
[2] School of Science, Huzhou University, Huzhou 313000, People's Republic of China
[3] Institute of Modern Physics, Chinese Academy of Sciences, Lanzhou 730000, People's Republic of China
[4] Joint Department for Nuclear Physics, Lanzhou University and Institute of Modern Physics, Chinese Academy of Sciences, Lanzhou 730000, People's Republic of China

E-mail: wangyongjia@zjhu.edu.cn and liqf@zjhu.edu.cn

Received 26 September 2019, revised 19 December 2019
Accepted for publication 30 December 2019
Published 12 February 2020

Abstract

The collision centrality (or the impact parameter b) in heavy-ion experiments is inferred from final state observables, however, usually b is an input to theoretical calculations. The effects of different methods used for the centrality selection (i.e. total charged multiplicity $M_{\rm ch}$, total transverse kinetic energy of light charged particles $E_{\perp 12}$, and the ratio of transverse-to-longitudinal kinetic energy *ERAT*) on the nuclear stopping and the collective flow are studied in ${}^{129}_{54}\mathrm{Xe}+{}^{120}_{50}\mathrm{Sn}$ collisions at INDRA energies ($E_{\rm beam} \leqslant 150$ MeV/nucleon). The study is conducted within the framework of the ultra-relativistic quantum molecular dynamics (UrQMD) model. It is found that the nuclear stopping power R_E obtained from events binning with *ERAT* is larger than the experimental data as well as the results obtained using $M_{\rm ch}$ and $E_{\perp 12}$. At $E_{\rm beam} = 50$ MeV/nucleon, the elliptic flow from events selected with different methods spreads widely, especially for more central collisions. The elliptic flow from events sorted by *ERAT* is weakly dependent on the collision centrality. The difference in elliptic flow at mid-rapidity among different centrality filters steadily decreases with increasing beam energy and impact parameter. At 150 MeV/nucleon, the differences in directed and elliptic flows arising from different centrality filters vanish.

[5] Authors to whom any correspondence should be addressed.

Keywords: heavy ion collisions, collective flow, nuclear stopping power, impact parameter

(Some figures may appear in colour only in the online journal)

1. Introduction

Understanding the properties of the dense and hot nuclear matter is one of the main purposes of heavy-ion collisions (HICs). The compressed nuclear matter formed in HICs exists only for a brief period of time, and direct experimental measurements of its properties are impossible to date. By using transport models to simulate the collision processes, one may deduce the properties of the compressed nuclear matter by comparing to the experimental data [1–7]. For a reliable result, theoretical calculations should be done with the same condition as in experiment, such as the collision centrality and the transverse momentum and rapidity windows.

In HICs, the impact parameter b, which characterizes the initial state of the collision, has a strong influence on the final state observables [8–13]. However, it can not be directly measured in experiments, but inferred from final state observables. For example, the total charged-particle multiplicity $M_{\rm ch}$ is found to be monotonically correlated to the centrality as in [14–20]. More central collisions are associated with larger $M_{\rm ch}$, as a gauge of the energy deposition. Another commonly used quantity is the total transverse kinetic energy of light charged particles (LCP) $E_{\perp 12}$ [22, 21, 23]. A larger magnitude of $E_{\perp 12}$ corresponds to a more central collision (see equation (5)). Another quantity is the ratio of transverse-to-longitudinal kinetic energy *ERAT*, adopted by the FOPI Collaboration as a criterion of the centrality [8, 24–27]. Similar to $E_{\perp 12}$, a larger value of *ERAT* denotes a more central collision. In addition, there are more approaches that have been applied by different experimental groups to infer the centrality at intermediate energies, such as the quadrupole momentum tensor along the beam direction Q_{zz} [28], the flow angle Θ_{flow} [1, 29], and the total kinetic-energy loss *TKEL* [30, 31].

In most theoretical studies, the impact parameter is the input variable. Recent studies emphasized that event selection methods used in experimental data analysis mix events with different impact parameters in a rather broad range [32–35]. Then the question arises: how do different centrality filters affect final observables, such as the collective flow and the nuclear stopping in HICs? To address the question, ^{129}Xe + ^{120}Sn collisions were simulated by the ultra-relativistic quantum molecular dynamics (UrQMD) model [36–38]. The stopping power and the collective flow from events binning with three commonly used impact parameter filters ($M_{\rm ch}$, $E_{\perp 12}$ and *ERAT*) are compared to those with the true impact parameter in the simulations.

The paper is organized as follows. In the next section, the UrQMD model, the observables, as well as the impact parameter filters are described briefly. The simulated results and the effects of centrality filters on observables are presented and discussed in section 3. Finally, a summary is given in section 4.

2. Model description and impact parameter filters

2.1. Model and observables

In the UrQMD model [39–41], each nucleon is represented by a coherent state of a Gaussian wave packet. The time evolution of the coordinate $\mathbf{r}_i$ and momentum $\mathbf{p}_i$ for each nucleon is

determined by Hamilton's equation of motion

$$\dot{\mathbf{r}}_i = \frac{\partial H}{\partial \mathbf{p}_i}, \quad \dot{\mathbf{p}}_i = -\frac{\partial H}{\partial \mathbf{r}_i}. \tag{1}$$

The Hamiltonian H consists of the kinetic energy T and the effective interaction potential energy U. Usually, the potential energy U depends on density (two-body and three-body Skyrme term), momentum (momentum-dependent term), and isospin asymmetry (symmetry energy term). In recent years, for a better description of experimental data at intermediate energies, the surface and the surface asymmetry energy terms from the Skyrme potential energy density functional are further introduced into the UrQMD model [39]. It is found, with a further consideration of a proper parameter set on the in-medium nucleon–nucleon cross section, that the existing collective flow and nuclear stopping data in HICs at intermediate energies can be reproduced reasonably well [38–42].

In HICs, the collective flow is frequently used to investigate the equation of state (EoS) of the nuclear matter. By expanding the azimuthal distribution of detected particles [43, 27], one obtain the directed v_1 and elliptic v_2 flows

$$v_1 \equiv \langle \cos\phi \rangle = \left\langle \frac{p_x}{p_\perp} \right\rangle = \left\langle \frac{p_x}{\sqrt{p_x^2 + p_y^2}} \right\rangle, \tag{2}$$

$$v_2 \equiv \langle \cos(2\phi) \rangle = \left\langle \frac{p_x^2 - p_y^2}{p_\perp^2} \right\rangle = \left\langle \frac{p_x^2 - p_y^2}{p_x^2 + p_y^2} \right\rangle, \tag{3}$$

where ϕ is the azimuthal angle, p_x and p_y are the components of the transverse momentum $p_\perp$. The angular brackets denote an average over all considered particles, summed over all events.

The nuclear stopping power which measures the energy converted from the beam direction (longitudinal) to the transverse direction is an important observable to characterize the collision dynamics at low as well as high energies [44, 26, 18, 28, 45, 25]. At INDRA energies ($\leqslant$150 MeV/nucleon), the quantity R_E, defined as the ratio of transverse to parallel energy, was introduced by the INDRA collaboration [18]. It reads as

$$R_E = \frac{1}{2} \frac{\sum_i^N E_{\perp i}}{\sum_i^N E_{\parallel i}}, \tag{4}$$

where $E_{\perp i}$ ($E_{\parallel i}$) is the transverse (parallel) kinetic energy of particles i in the center-of-mass frame [18], and the summation is taken over the total number N of reaction products.

2.2. Impact parameter filters

In UrQMD calculations [46, 48, 49, 47, 50], the impact parameter b for each event can be sampled from $b_{\min}$ to $b_{\max}$ with bdb weighted distribution. Where $b_{\max} = (R_T + R_P)$ fm, R_T and R_P are the radii of target and projectile nuclei, respectively. For each event, the true impact is precisely known. In the present work, three different methods in the estimation of the impact parameter frequently used by experiments, were studied and compared with the true impact parameter used in model calculations.

(i) The total charged multiplicity $M_{\rm ch}$. It is based on the assumption that the multiplicity dependence of the measured cross section is interpreted as an impact parameter dependence of the geometrical reaction cross section [15]. One can estimate impact parameter from a monotonic relation between $M_{\rm ch}$ and b [17, 35]:

$$b_{\rm est}(M_{\rm ch} \geqslant M'_{\rm ch}) = b_{\rm max} \cdot \left(\frac{\sum_{M'_{\rm ch}}^{\infty} \sigma(M_{\rm ch})}{\sum_{0}^{\infty} \sigma(M_{\rm ch})} \right)^{1/2},$$

$$= b_{\rm max} \cdot \left(\frac{\sum_{M'_{\rm ch}}^{\infty} N(M_{\rm ch})}{\sum_{0}^{\infty} N(M_{\rm ch})} \right)^{1/2}$$

$$\bar{b}_{\rm est}(M_{\rm ch} \geqslant M'_{\rm ch}) = \frac{1}{2}[b_{\rm est}(M'_{\rm ch} + 1) + b_{\rm est}(M'_{\rm ch} - 1)], \tag{5}$$

where $\sigma(M_{\rm ch})$ and $N(M_{\rm ch})$ are the cross section and the number of events with the charge multiplicity equal to $M_{\rm ch}$, respectively. For a given value of $M'_{\rm ch}$, the estimated impact parameter $\bar{b}_{\rm est}$ with $M_{\rm ch} \geqslant M'_{\rm ch}$ can be approximately determined by equation (5). For example, in [21], $M_{\rm ch} \geqslant 55$ was used to select central events ($b \leqslant 1.5$ fm) for ^{197}Au $+^{197}$Au at 60 MeV/nucleon.

(ii) The transverse kinetic energy ($E_{\perp 12}$) of LCP is defined as [22]

$$E_{\perp 12} = \sum_{Z=1,2} \frac{p_{\perp}^2}{2m}, \tag{6}$$

where m is the mass of considered LCP, and the summation is taken over the particles with $Z = 1$ and $Z = 2$ only. In [22, 23], the spectrum of $E_{\perp 12}$ was divided into eight bins to illustrate the relation between $E_{\perp 12}$ and the impact parameter. This is done by using the following geometrical prescription:

$$b_{\rm est}(E_{\perp 12} \geqslant E'_{\perp 12}) = b_{\rm max} \cdot \left(\frac{\int_{E'_{\perp 12}}^{\infty} N(E_{\perp 12})}{\int_{0}^{\infty} N(E_{\perp 12})} \right)^{1/2},$$

$$\bar{b}_{\rm est}(E_{\perp 12} \geqslant E'_{\perp 12}) = \frac{1}{2}[b_{\rm est}(E'_{\perp 12} + 0.01) + b_{\rm est}(E'_{\perp 12} - 0.01)]. \tag{7}$$

Here $N(E_{\perp 12})$ is the number of events with $E_{\perp 12}$ equal to a certain value. For example, in [21], the INDRA and ALADIN Collaborations selected central events ($b/b_{\rm max} \leqslant 0.1$) for ^{197}Au $+^{197}$Au at 60 MeV/nucleon by $E_{\perp 12} \geqslant 1.256$ GeV.

(iii) The ratio of total transverse to longitudinal kinetic energy in the center-of-mass system (*ERAT*), which is frequently adopted by FOPI Collaboration [8, 25–27], defined as

$$ERAT = \frac{E_{\perp}}{E_{\parallel}} = \frac{\sum_i [p_{\perp i}^2 / (2Z_i m + E_i)]}{\sum_i [p_{\parallel i}^2 / (2Z_i m + E_i)]}, \tag{8}$$

the definition of $E_{\perp}$, $E_{\parallel}$, $p_{\perp}$, and m are the same as the above description. And $p_{\parallel}$, Z and E are the longitudinal momentum, charge number and the total energy of a fragment,

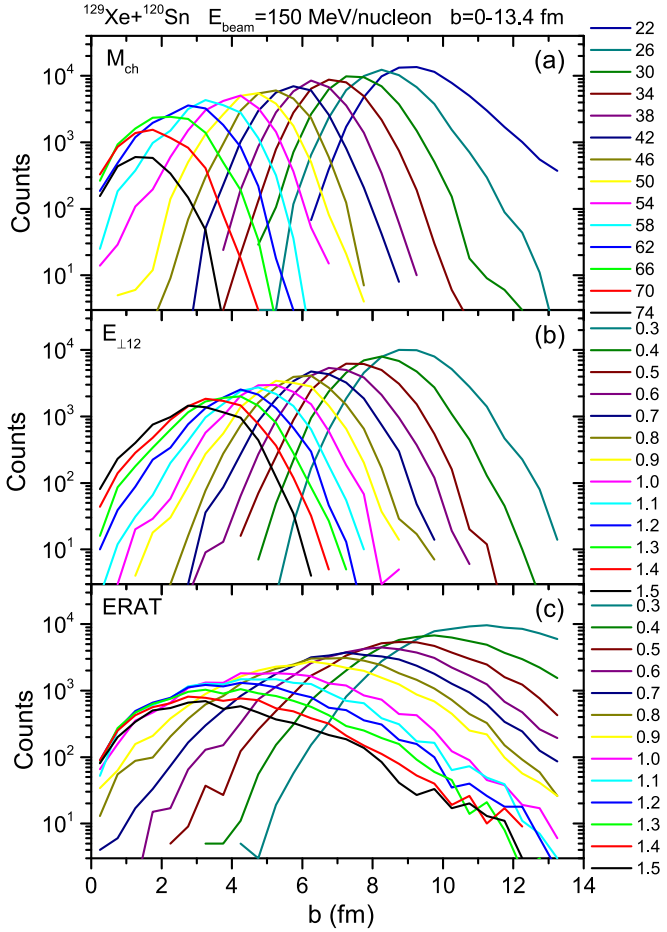

Figure 1. The impact parameter distributions for events with fixed $M_{\rm ch}$ (a), $E_{\perp 12}$ (b) and *ERAT* (c). All results are obtained from ^{129}Xe+^{120}Sn collisions at $E_{\rm beam}$ = 150 MeV/nucleon with b = 0–13.4 fm.

respectively. In this work, only free protons are considered for simplicity. The impact parameter b can be estimate from the distribution of the *ERAT*, using a geometrical sharp-cut approximation:

$$b_{\rm est}(ERAT \geqslant ERAT') = b_{\rm max} \cdot \left(\frac{\int_{ERAT'}^{\infty} N(ERAT)}{\int_{0}^{\infty} N(ERAT)} \right)^{1/2},$$

$$\bar{b}_{\rm est}(ERAT \geqslant ERAT') = \frac{1}{2}[b_{\rm est}(ERAT' + 0.01) + b_{\rm est}(ERAT' - 0.01)]. \quad (9)$$

Here N (*ERAT*) is the number of events with *ERAT* equal to a certain value. For example, in [8], $ERAT \geqslant 0.69$ was adopted by FOPI Collaboration to choose central events ($b < 3$ fm) for ^{197}Au +^{197}Au at 150 MeV/nucleon. We note that *ERAT* selection was usually used by FOPI Collaboration for studies of HICs at beam energies above 100 MeV/nucleon.

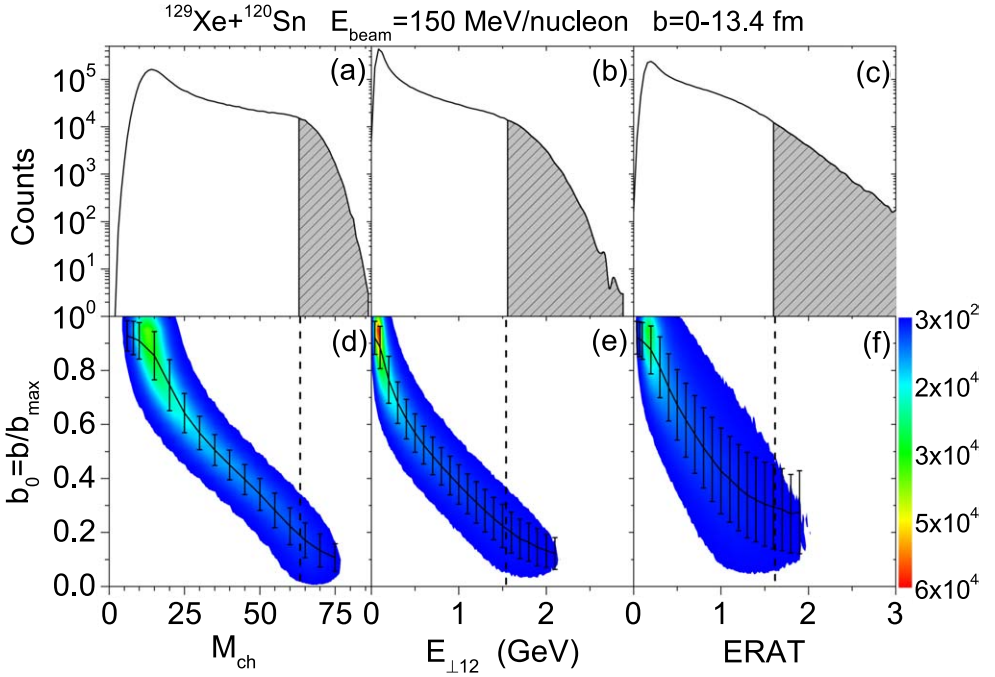

Figure 2. Top panels: the distributions of the total multiplicity of charged particles $M_{\rm ch}$ (a), the total transverse kinetic energy of light charged particles $E_{\perp 12}$ (b) and the ratio of total transverse to longitudinal kinetic energy *ERAT* (c) for ^{129}Xe+^{120}Sn at 150 MeV/nucleon. The estimated impact parameter $\bar{b}_{\rm est} \leqslant 2.6$ fm corresponds to $M_{\rm ch} \geqslant 63$, $E_{\perp 12} \geqslant 1.58$ GeV and $ERAT \geqslant 1.6$, respectively (hatched areas). Lower panels: the correlations between the reduced impact parameter $b_0 = b/b_{\rm max}$ and $M_{\rm ch}$ (d), $E_{\perp 12}$ (e), as well as *ERAT* (f).

To reveal the relationship between the true impact parameter (which means the input impact parameter b for model calculations) and $M_{\rm ch}$, $E_{\perp 12}$, as well as *ERAT*, figure 1 presents the distributions of the impact parameter of simulated events sorted by different filters from ^{129}Xe+^{120}Sn at 150 MeV/nucleon collisions with the true impact parameter varies from 0 to $b_{\rm max} = 13.4$ fm. As shown, the true impact parameter has a wide distribution for each selection. Thus, there does not exist a strictly one-to-one relationship between the impact parameter and $M_{\rm ch}$, $E_{\perp 12}$, $M_{\rm ch}$ [14, 15]. For example, for the most central events with $M_{\rm ch} = 74$, the range of the true impact parameter b varies from 0 to 6.5 fm. For $E_{\perp 12} = 1.5$ GeV and $ERAT = 1.5$, the corresponding true impact parameters fall in range of $0 < b < 6$ fm and $0 < b < 12$ fm, respectively. With a larger value of $M_{\rm ch}$, $E_{\perp 12}$, or *ERAT*, the peak of each line is gradually shifted toward smaller impact parameter as expected.

The counts of simulated events (top panels) and the reduced impact parameter $b_0 = b/b_{\rm max}$ (bottom panels) as a function of $M_{\rm ch}$ ((a) and (d)), $E_{\perp 12}$ ((b) and (e)) and *ERAT* [(c) and (f)], respectively, are shown in figure 2. The solid line with error bars in panels (d), (e) and (f), respectively, indicates the mean value of b_0, where the error bar indicates are standard deviation. The dashed line $M_{\rm ch} = 63$, $E_{\perp 12} = 1.58$ GeV and $ERAT = 1.6$ are obtained with the geometric prescription defined in equation (5), (7) and (9), corresponding to the estimated impact parameter $\bar{b}_{\rm est} = 2.6$ fm. This means that collision events with $M_{\rm ch} \geqslant 63$, $E_{\perp 12} \geqslant 1.58$ GeV, or $ERAT \geqslant 1.6$ are selected as the central events corresponding to the same cross section with $b \leqslant 2.6$ fm for ^{129}Xe +^{120}Sn collisions at $E_{\rm beam} = 150$ MeV/nucleon. The

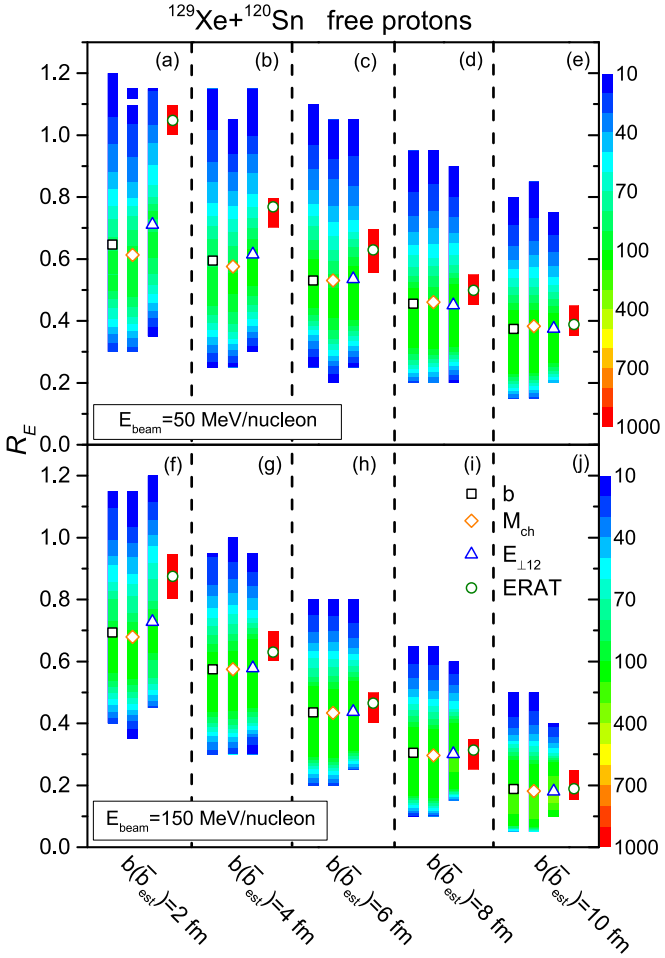

Figure 3. Bidimensional distributions of the nuclear stopping power R_E of the events selected by different impact parameter filters at 50 MeV/nucleon (top panels) and 150 MeV/nucleon (bottom panels). The scatter represent the mean value of R_E of the events selected by b (black squares), $M_{\rm ch}$ (orange diamonds), $E_{\perp 12}$ (blue triangles) and *ERAT* (olive circles).

corresponding relationship between the true impact parameter and $M_{\rm ch}$, $E_{\perp 12}$ and *ERAT* at several beam energies between 50 to 150 MeV/nucleon are listed in Appendix. In addition, one can notice that for central collisions, with a certain impact parameter, $M_{\rm ch}$ has smaller fluctuation and narrower distribution than those of $E_{\perp 12}$ and *ERAT*. For a fixed value of *ERAT*, the distribution of the true impact parameter has the broadest range.

3. Results and discussions

3.1. Nuclear stopping power

The impact parameter dependence of the stopping observable R_E for free protons emitted in ^{129}Xe+^{120}Sn collisions are shown in figure 3. Results obtained with $M_{\rm ch}$, $E_{\perp 12}$, *ERAT* are

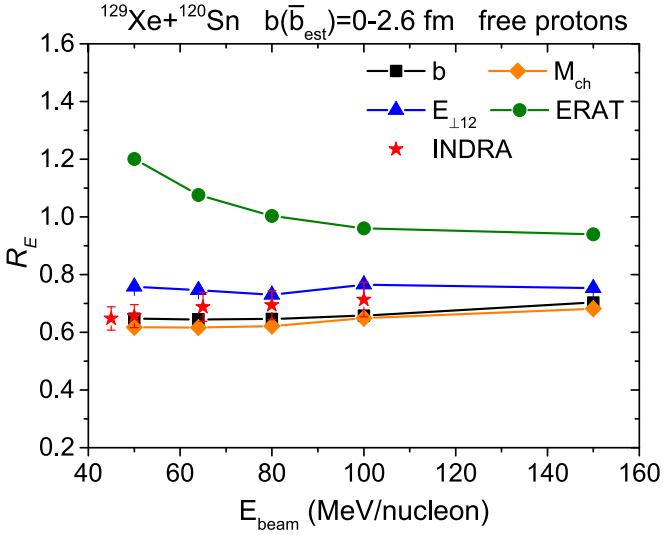

Figure 4. Beam energy dependence of the nuclear stopping power R_E of free protons in central ^{129}Xe+^{120}Sn collisions ($b \leqslant 2.6$ fm). Simulated with four centrality filters, the true impact parameter (black line with squares), $M_{\rm ch}$ (orange line with diamonds),$E_{\perp 12}$ (blue line with triangles) and *ERAT* (olive line with circles), are compared with the experimental data from the INDRA Collaboration ($M_{\rm ch}$ was adopted).

compared with the one with the true impact parameter. As shown in the contour plots, the distribution of R_E of the events selected by $M_{\rm ch}$ or $E_{\perp 12}$ is similar to that of the events with true impact parameter. However, the stopping of the events selected by *ERAT* have the minimal width, and the mean value is larger than that obtained from other filters, especially for small impact parameter collisions. The difference in R_E obtain with different filters decreases with increasing b and increasing beam energy. In addition, all results obtained with different centrality filters showed that the stopping power decreases with increase b, as expected.

To present more clearly the influence of different centrality filter on nuclear stopping at INDRA energies, the beam energy dependence of the nuclear stopping power R_E of free protons produced in central ($b \leqslant 2.6$ fm) ^{129}Xe+^{120}Sn collisions are shown in figure 4. It can be seen again that R_E obtained from the true impact parameter and $M_{\rm ch}$ lie close to each other and well reproduce the INDRA experimental data ($M_{\rm ch}$ was adopted) [19], the result from $E_{\perp 12}$ is slightly larger than the data, but those obtained by using *ERAT* apparently overestimate the data. This is because the autocorrelation between R_E and *ERAT*. From equations (4) and (9), for a certain event and a certain particle species, $R_E = \frac{1}{2}ERAT$ in the non-relativistic limit. In addition, $E_{\perp 12}$ and R_E are also partly correlated since both of them contains the transverse kinetic energy. By using $E_{\perp 12}$ and *ERAT* filters, events which have larger transverse energy (more energy is converted from the longitudinal direction) are more likely to be selected as central collisions, thus give larger value of R_E. To avoid the autocorrelations, $E_{\perp 12}$ and *ERAT* filters ought not to be used to study R_E, especially for central collision. In [33], it has been shown that, although the events with high multiplicity have a broad impact parameter range, it would have a small effect on the observable R_E.

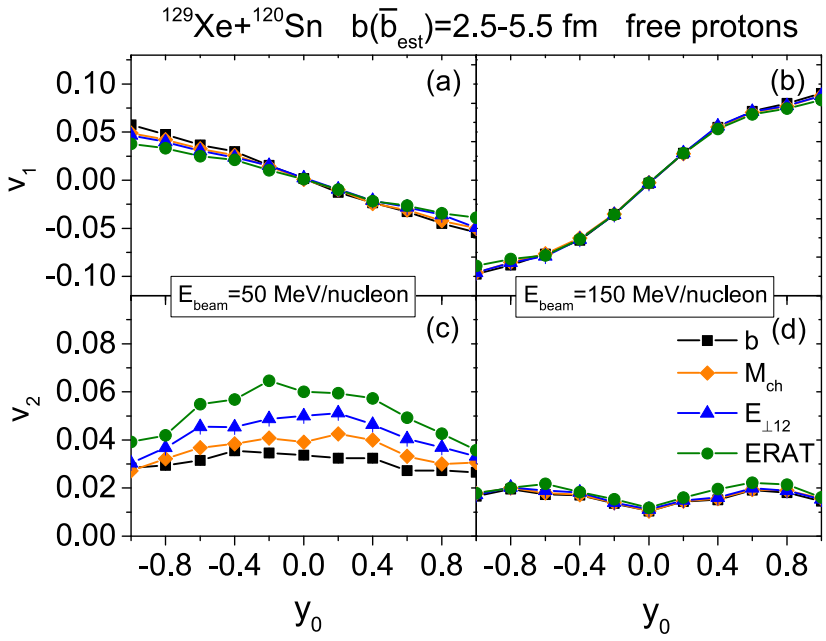

Figure 5. The directed flow v_1 ((a)and (b)) and elliptic flow v_2 ((c) and (d)) of protons as a function of reduced rapidity $y_0(=y_z/y_{pro})$ for ^{129}Xe +^{120}Sn at the beam energies 50 and 150 MeV/nucleon, respectively. The impact parameter $b(\bar{b}_{est})$ = 2.5–5.5 fm is adopted.

3.2. Directed and elliptic flows

Figure 5 displays the collective flow of free protons as a function of the reduced rapidity ($y_0 = y_z/y_{pro}$) for ^{129}Xe +^{120} Sn collisions at 50 and 150 MeV/nucleon with impact parameter of 2–5.5 fm. The directed flow parameter v_1 and elliptic flow parameter v_2 from events binned with M_{ch}, $E_{\perp 12}$ and *ERAT* are compared to the results with the true impact parameter b = 2.5–5.5 fm. At E_{beam} = 150 MeV/nucleon, both v_1 and v_2 values obtained with different filters lie close to each other, while at E_{beam} = 50 MeV/nucleon, the discrepancy among the values with different filters can be clearly observed, especially for the elliptic flow. The value of v_2 obtained from *ERAT* and $E_{\perp 12}$ are larger than that with M_{ch} and the true impact parameter. As we have known, the positive v_2 means nucleons more likely undergo an in-plane emission rather than an out-of-plane pattern. A larger transverse energy in the cases of *ERAT* and $E_{\perp 12}$ results in a stronger in-plane emission.

To quantitatively evaluate the influence of impact parameter filters on the elliptic flow, the v_2 at mid-rapidity for free protons as a function of impact parameters is shown in figure 6. Similar to the results shown in figure 5, the differences in v_2 at 150 MeV/nucleon are minor, while obvious differences can be observed at 50 MeV/nucleon, especially with smaller impact parameter. The v_2 from events selected by both $E_{\perp 12}$ and *ERAT* show a weak dependence on impact parameter. This is because events selected by $E_{\perp 12}$ or *ERAT* are highly mixed over a rather broad range of the true impact parameters, as can be seen in figure 2.

Furthermore, the influence of impact parameter filters on v_2 at higher beam energies (i.e. 250 and 400 MeV/nucleon) are studied as well. The excitation function of the v_2 at mid-rapidity for free protons from ^{129}Xe +^{120} Sn collisions with various impact parameter regions

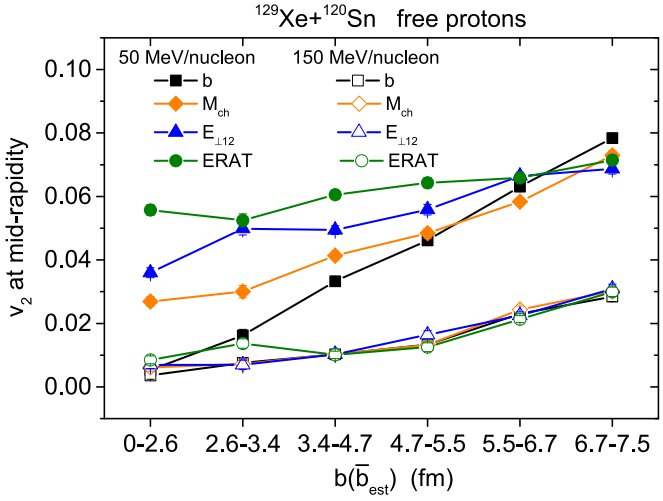

Figure 6. Impact parameter dependence of the v_2 at mid-rapidity for free protons from ^{129}Xe +^{120}Sn collisions at the beam energies 50 (solid symbols) and 150 (open symbols) MeV/nucleon, respectively.

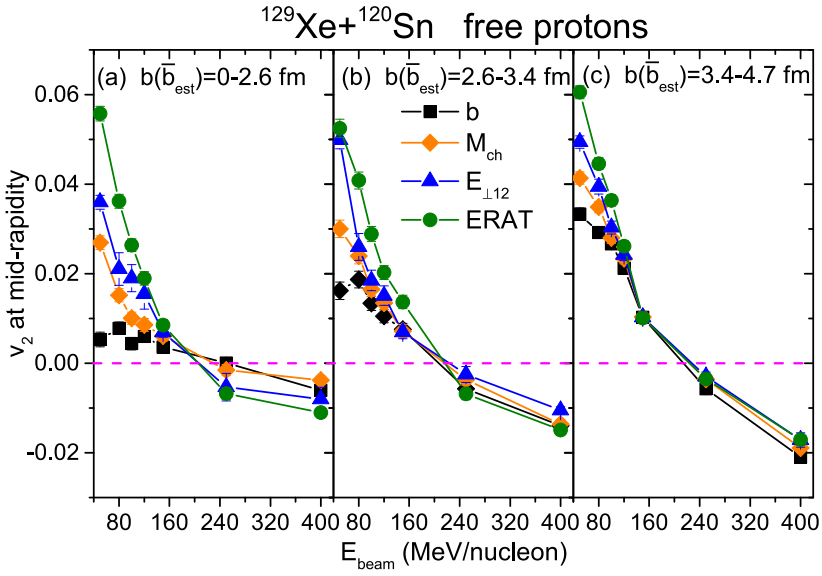

Figure 7. The v_2 of free protons at mid-rapidity ($|y_z/y_{pro}| < 0.1$) as a function of the beam energy (40–400 MeV/nucleon) from ^{129}Xe +^{120}Sn collisions at impact parameter $b(\bar{b}_{est})$ = 0–2.6 fm (left), 2.6–3.4 fm (middle), 3.4–4.7 fm (right).

are presented in figure 7. As expected, no matter which filter being used, the elliptic flow v_2 decreases with increasing beam energy and changes sign at a particular beam energy, which is called transition energy [26, 53–55]. The change of sign of v_2 reflects the transition from an enhanced in-plane ($v_2 > 0$) to a preferential out-of-plane ($v_2 < 0$) emission. This phenomenon can be attributed to a change from a collective rotating motion governed by the attractive

mean field at low energies, to the collective expansion (squeeze-out scenario) resulting from the repulsive pressure at high density stage at high energies [56]. It is further found that the transition energy is not very sensitive to the chosen of the impact parameter filter, as the v_2 is approaching zero at the transition energy. At the energies below the transition energy, the difference in v_2 among different centrality filters decreases with increasing beam energy, and distinct difference can be observed at $E_{\rm beam} \lesssim 100$ MeV/nucleon. While above the transition energy, the absolute value of v_2 increases with increasing beam energy, the effect of impact parameter filters on v_2 emerges again. At higher energies, other methods (such as the forward energy E_F [51] and the number of participating nucleons $N_{\rm part}$ [52]) are also used to determine centrality, the influence of these methods on various observables deserves further detailed investigation. In addition, the observed effect of centrality filters on v_2 is more pronounced at small centrality than that at large impact parameter, which is similar as observed in figure 6.

4. Summary

We evaluate the influence of impact parameter filters, the total charged multiplicity $M_{\rm ch}$, the total transverse kinetic energy of light charged particles $E_{\perp 12}$ and the ratio of transverse-to-longitudinal kinetic energy (*ERAT*), on the collective flow and the nuclear stopping power. These observables are obtained from ^{129}Xe + ^{120}Sn collisions within the UrQMD model. It is found that there is not a strictly one-to-one relationship between impact parameter and $M_{\rm ch}$, $E_{\perp 12}$ or *ERAT*. The distribution of the true impact parameters of events selected by a fixed *ERAT* has the broadest range, while that by $M_{\rm ch}$ covers a relatively narrow range. Both the collective flow and the nuclear stopping power obtained from events sorted by $M_{\rm ch}$ lie closely to that by the true impact parameter. Due to the autocorrelation between *ERAT* and R_E, the R_E of central collision events selected by *ERAT* is overestimated, compared to the experimental data. At 50 MeV/nucleon, the elliptic flow from events selected by different methods spread widely, especially for more central impact parameters. The elliptic flow from events sorted by *ERAT* is found to be weakly sensitive to the collision centrality. Further, it is interesting to see that at beam energies below the transition energy (here, ∼200 MeV/nucleon), the difference in elliptic flow at mid-rapidity among different centrality filters steadily decreases with increasing beam energy and impact parameter. While at beam energies above the transition energy, the absolute value of v_2 increases with increasing beam energy, the influence of impact parameter filters on v_2 can be observed again.

Acknowledgments

We thank Professor F Q Wang for valuable discussions and and revisions of this manuscript. The computational calculations of this work are performed by using the C3S2 in Huzhou University. This work is supported by the National Natural Science Foundation of China under Grants No. 11947410, No. 11875125, No. 11847315, No. 11675066, and the Zhejiang Provincial Natural Science Foundation of China under Grants No. LY18A050002 and No. LY19A050001, and the 'Ten Thousand Talent Program' of Zhejiang province.

Appendix. The impact parameter estimated with filters $M_{\rm ch}$, $E_{\perp 12}$ or *ERAT*

The estimated impact parameter $\bar{b}_{\rm est}$ versus the observables $M_{\rm ch}$, $E_{\perp 12}$ and *ERAT* in the beam energy range of 50-150 MeV/nucleon are tabulated in tables A1–A3, respectively. The

Table A1. The estimated impact parameter from the total charged multiplicity $M_{\rm ch}$ by equation (5).

$M_{\rm ch}$	50 $\bar{b}_{\rm est}$	64 $\bar{b}_{\rm est}$	80 $\bar{b}_{\rm est}$	100 $\bar{b}_{\rm est}$	150 (MeV/nucleon) $\bar{b}_{\rm est}$ (fm)
8	13.4	13.4	13.4	13.4	13.3
10	13.4	13.3	13.3	13.3	13.1
12	13.3	13.2	13.1	13.0	12.7
14	13.0	12.9	12.8	12.5	12.0
16	12.6	12.5	12.2	11.9	11.2
18	12.1	11.8	11.5	11.1	10.4
20	11.4	11.1	10.8	10.4	9.8
22	10.6	10.4	10.1	9.8	9.2
24	9.8	9.7	9.4	9.2	8.7
26	9.1	9.0	8.8	8.6	8.3
28	8.3	8.3	8.3	8.1	7.9
30	7.5	7.7	7.7	7.7	7.6
32	6.7	7.1	7.2	7.2	7.2
34	5.9	6.5	6.7	6.8	6.9
36	5.1	5.9	6.3	6.4	6.6
38	4.2	5.3	5.8	6.0	6.3
40	3.4	4.6	5.3	5.7	6.0
42	2.6	4.0	4.8	5.3	5.7
44	1.9	3.3	4.3	4.9	5.5
46	1.3	2.7	3.8	4.5	5.2
48	0.8	2.1	3.3	4.1	4.9
50	0.5	1.5	3.7	3.7	4.6
52	0.3	1.1	2.2	3.2	4.3
54	0.2	0.7	1.7	2.8	4.0
56	0.1	0.4	1.3	2.3	3.7
58		0.3	0.9	1.8	3.4
60		0.1	0.6	1.4	3.1
62			0.4	1.1	2.7
64			0.2	0.7	2.4
66			0.1	0.5	2.0
68				0.3	1.6
70				0.2	1.3

Table A2. The estimated impact parameter from the transverse kinetic energy $E_{\perp 12}$ by equation (7).

$E_{\perp 12}$ (GeV)	50 $\bar{b}_{\rm est}$	64 $\bar{b}_{\rm est}$	80 $\bar{b}_{\rm est}$	100 $\bar{b}_{\rm est}$	150 (MeV/nucleon) $\bar{b}_{\rm est}$ (fm)
0.10	12.9	12.8	12.7	12.5	12.1
0.15	11.8	11.6	11.4	11.2	10.9
0.20	10.2	10.2	10.2	10.1	10.1
0.25	8.7	9.0	9.2	9.3	9.5
0.30	7.1	7.9	8.3	8.6	9.0
0.35	5.6	6.8	7.5	8.0	8.6
0.40	4.3	5.8	6.8	7.4	8.2

Table A2. (Continued.)

$E_{\perp 12}$ (GeV)	50 $\bar{b}_{\rm est}$	64 $\bar{b}_{\rm est}$	80 $\bar{b}_{\rm est}$	100 $\bar{b}_{\rm est}$	150 (MeV/nucleon) $\bar{b}_{\rm est}$ (*fm*)
0.45	3.0	4.8	6.1	6.9	7.9
0.50	2.0	3.9	5.4	6.4	7.5
0.55	1.3	3.0	4.7	5.9	7.2
0.60	0.8	2.3	4.1	5.5	7.0
0.65	0.4	1.7	3.5	5.0	6.7
0.70	0.2	1.1	2.9	4.6	6.4
0.75	0.1	0.8	2.3	4.1	6.2
0.80		0.5	1.8	3.7	5.9
0.85		0.3	1.4	3.3	5.7
0.90		0.2	1.1	2.9	5.5
0.95		0.1	0.8	2.5	5.2
1.00			0.6	2.1	5.0
1.10			0.3	1.4	4.6
1.20			0.1	0.9	4.2
1.30				0.5	3.7
1.40				0.3	3.3
1.50				0.1	2.9
1.60					2.5
1.70					2.1

Table A3. The estimated impact parameter from the ratio of transverse-to-longitudinal kinetic energy *ERAT* by equation (9).

ERAT	50 $\bar{b}_{\rm est}$	64 $\bar{b}_{\rm est}$	80 $\bar{b}_{\rm est}$	100 $\bar{b}_{\rm est}$	150 (MeV/nucleon) $\bar{b}_{\rm est}$ (*fm*)
0.1	13.4	13.4	13.4	13.4	13.3
0.2	13.4	13.3	13.3	13.1	12.3
0.3	13.2	13.0	12.7	12.1	10.9
0.4	12.9	12.4	11.8	11.0	9.9
0.5	12.3	11.5	10.7	10.0	9.1
0.6	11.5	10.6	9.7	9.0	8.3
0.7	10.6	9.6	8.8	8.1	7.6
0.8	9.7	8.7	7.9	7.3	6.9
0.9	8.8	7.7	7.0	6.6	6.3
1.0	7.9	6.9	6.2	5.8	5.6
1.1	7.1	6.1	5.5	5.2	5.0
1.2	6.3	5.4	4.9	4.5	4.4
1.3	5.6	4.8	4.3	4.0	3.9
1.4	5.0	4.2	3.7	3.5	3.4
1.5	4.5	3.7	3.3	3.0	2.9
1.6	4.0	3.3	2.8	2.6	2.5
1.7	3.5	2.9	2.5	2.3	2.2
1.8	3.1	2.5	2.2	1.9	1.9
1.9	2.8	2.2	1.9	1.7	1.6
2.0	2.5	2.0	1.7	1.5	1.4
2.1	2.2	1.7	1.4	1.3	1.2
2.2	2.0	1.5	1.3	1.1	1.0

simulations were performed in the full impact parameter range of the ^{129}Xe + ^{120}Sn reactions, i.e. $b = 0-13.4$ fm, by utilizing UrQMD model.

ORCID iDs

Pengcheng Li https://orcid.org/0000-0002-7750-4034
Hongfei Zhang https://orcid.org/0000-0003-0326-5701

References

[1] Stöcker H and Greiner W 1986 *Phys. Rep.* **137** 277
[2] Danielewicz P, Lacey R and Lynch W G 2002 *Science* **298** 1592
[3] Li B A, Chen L W and Ko C M 2008 *Phys. Rep.* **464** 113
[4] Aichelin J 1991 *Phys. Rep.* **202** 233
[5] Lü L M, Yi H, Xiao Z G, Shao M, Zhang S, Xiao G Q and Xu N 2017 *Sci. China-Phys. Mech. Astron.* **60** 012021
[6] Ono A 2019 *Prog. Part. Nucl. Phys.* **105** 139
[7] Xu J 2019 *Prog. Part. Nucl. Phys.* **106** 312
[8] Reisdorf W *et al* (FOPI Collaboration) 1997 *Nucl. Phys.* A **612** 493
[9] Tsang M B, Bertsch G F, Lynch W G and Tohyama M 1989 *Phys. Rev.* C **40** 1685
[10] Tsang M B *et al* 2004 *Phys. Rev. Lett.* **92** 062701
[11] Galichet E *et al* (INDRA Collaboration) 2009 *Phys. Rev.* C **79** 064614
[12] Sun Z Y *et al* 2010 *Phys. Rev.* C **82** 051603
[13] Zhang Y X, Coupland D D S, Danielewicz P, Li Z X, Liu H, Lu F, Lynch W G and Tsang M B 2012 *Phys. Rev.* C **85** 024602
[14] Ogilvie C A, Cebra D A, Clayton J, Howden S, Karn J, Vander Molen A, Westfall G D, Wilson W K and Winfield J S 1989 *Phys. Rev.* C **40** 654
[15] Cavata C, Demoulins M, Gosset J, Lemaire M C, L'Hôte D, Poitou J and Valette O 1990 *Phys. Rev.* C **42** 1760
[16] Tsang M B, de Souza R T, Kim Y D, Bowman D R, Carlin N, Gelbke C K, Gong W G, Lynch W G, Phair L and Zhu F 1991 *Phys. Rev.* C **44** 2065
[17] Kim Y D, de Souza R T, Bowman D R, Carlin N, Gelbke C K, Gong W G, Lynch W G, Phair L, Tsang M B and Zhu F 1992 *Phys. Rev.* C **45** 338
[18] Lehaut G *et al* (INDRA Collaboration and ALADIN Collaborations) 2010 *Phys. Rev. Lett.* **104** 232701
[19] Lopez O *et al* (INDRA Collaboration) 2014 *Phys. Rev.* C **90** 064602
[20] Phair L *et al* 1992 *Nucl. Phys.* A **548** 489
[21] Le Fèvre A *et al* (INDRA and ALADIN Collaborations) 2004 *Nucl. Phys.* A **735** 219
[22] Łukasik J *et al* 1997 *Phys. Rev.* C **55** 1906
[23] Plagnol E *et al* (INDRA Collaborations) 1999 *Phys. Rev.* C **61** 014606
[24] Kuhn C *et al* 1993 *Phys. Rev.* C **48** 1232
[25] Reisdorf W *et al* (FOPI Collaborations) 2004 *Phys. Rev. Lett.* **92** 232301
[26] Andronic A, Lukasik J, Reisdorf W and Trautmann W 2006 *Eur. Phys. J.* A **30** 31
[27] Reisdorf W *et al* (FOPI Collaborations) 2012 *Nucl. Phys.* A **876** 1
[28] Bauer W 1988 *Phys. Rev. Lett.* **61** 2534
[29] Frankland J D *et al* (INDRA Collaborations) 2001 *Nucl. Phys.* A **689** 905
[30] Charity R J *et al* 1991 *Z. Phys.* A **341** 53
[31] Piantelli S, Bidini L, Poggi G, Bini M, Casini G, Maurenzig P R, Olmi A, Pasquali G, Stefanini A A and Taccetti N 2002 *Phys. Rev. Lett.* **88** 052701
[32] Zhang G Q, Ma Y G, Cao X G, Zhou C L, Cai X Z, Fang D Q, Tian W D and Wang H W 2011 *Phys. Rev.* C **84** 034612
[33] Bonnet E, Colonna M, Chbihi A, Frankland J D, Gruyer D and Wieleczko J P 2014 *Phys. Rev.* C **89** 034608
[34] Basrak Z, Eudes P and de la Mota V 2016 *Phys. Rev.* C **93** 054609
[35] Li L, Zhang Y X, Li Z X, Wang N, Cui Y and Winkelbauer J 2018 *Phys. Rev.* C **97** 044606

[36] Bass S A *et al* 1998 *Prog. Part. Nucl. Phys.* **41** 255
[37] Bleicher M *et al* 1999 *J. Phys. G: Nucl. Part. Phys.* **25** 1859
[38] Li Q F, Shen C W, Guo C C, Wang Y J, Li Z X, Lukasik J and Trautmann W 2011 *Phys. Rev.* C **83** 044617
[39] Wang Y J, Guo C C, Li Q F, Zhang H F, Leifels Y and Trautmann W 2014 *Phys. Rev.* C **89** 044603
Wang Y J, Guo C C, Li Q F, Zhang H F, Li Z X and Trautmann W 2014 *Phys. Rev.* C **89** 034606
Wang Y J, Guo C C, Li Q F, Li Z X, Su J and Zhang H F 2016 *Phys. Rev.* C **94** 024608
[40] Li P C, Wang Y J, Li Q F, Guo C C and Zhang H F 2018 *Phys. Rev.* C **97** 044620
[41] Wang Y J, Guo C C, Li Q F, Le Fèvre A, Leifels Y and Trautmann W 2018 *Phys. Lett.* B **778** 207
[42] Liu Y Y, Wang Y J, Li Q F and Liu L 2018 *Phys. Rev.* C **97** 034602
[43] Reisdorf W and Ritter H G 1997 *Ann. Rev. Nucl. Part. Sci.* **47** 663
[44] Hong B *et al* (FOPI Collaboration) 2002 *Phys. Rev.* C **66** 034901
[45] Liu J Y, Guo W J, Wang S J, Zuo W, Zhao Q and Yang Y F 2001 *Phys. Rev. Lett.* **86** 975
[46] Petersen H, Li Q F, Zhu X L and Bleicher M 2006 *Phys. Rev.* C **74** 064908
[47] Li P C, Wang Y J, Li Q F and Zhang H F 2018 *Nucl. Sci. Tech.* **29** 177
[48] Du Y S, Wang Y, Li Q F and Liu L 2018 *Sci. China Phys. Mech. Astron* **61** 062011
[49] Li Q F, Wang Y J, Wang X B and Shen C W 2016 *Sci. China-Phys. Mech. Astron* **59** 632002
[50] Zou L Y, Li M, Guo C C, Wang Y J, Li Q F and Liu L 2016 *Sci. China-Phys. Mech. Astron* **59** 122011
[51] Motornenko A, Begun V V, Vovchenko V, Gorenstein M I and Stoecker H 2019 *Phys. Rev.* C **99** 034909
[52] Miller M L, Reygers K, Sanders S J and Steinberg P 2007 *Annu. Rev. Nucl. Part. Sci* **57** 205
[53] Andronic A *et al* (FOPI Collaboration) 2001 *Nucl. Phys.* A **679** 765
[54] Andronic A *et al* (FOPI Collaboration) 2005 *Phys. Lett.* B **612** 173
[55] Łukasik J *et al* (INDRA and ALADIN Collaborations) 2005 *Phys. Lett.* B **608** 223
[56] Crochet P *et al* (FOPI Collaboration) 1997 *Nucl. Phys.* A **624** 755